A Predictive Model for Life Assessment of Automotive Exhaust Mufflers Subject to Internal Corrosion Failure due to Exhaust Gases Condensation

M. H. Nazir [1], Z. A. Khan [1], A. Saeed [1], K. Stokes [2]

[1] Bournemouth University
Sustainable Design Research Cluster (SDRC)
Faculty of Science and Technology, BH12 5BB, UK
[2] Defence Science and Technology Labs (DSTL), Salisbury, UK

Abstract

A study has been presented of pitting corrosion on internal walls of automotive exhaust muffler due to exhaust gases condensation. The problem mainly exists in the rear section of exhaust system close to tail end pipe such as muffler, especially when the temperature of muffler does not go up during short distance run or winter. The water vapor condenses on the muffler's inner wall in the form of water droplets. The dissolution of corrosive gases which are coming from internal combustion of engine as well as condensation of low-pH acidic vapors in the water droplet can cause severe pitting corrosion on standard exhaust steel. In this work, an experiment is reported for internal corrosion, by using mufflers as test bed subjected to different environmental conditions. Based on observations, a mechanistic model has been developed which involves three main techniques (i) the dropwise condensation technique predicts the condensation rate and is based on heat and mass transfer theory (ii) the species breakdown in the droplet is established through the main thermodynamic and chemical equilibrium (iii) the pitting corrosion involving pit depth is predicted using electrochemical kinetic reactions, species transport and chemical reactions occurring inside the droplet. Lastly, the accuracy of model has been validated by comparison between experimental and predicted results showing a good agreement

Keywords: Automotive exhaust system, muffler, condensation, pitting corrosion, predictive modelling

1 Introduction

Modern automotive exhaust systems consist of several individual sections from engine side to the tail end pipe. The material properties of these sections directly relate with the operating temperature to which each section is submitted, ranging from 600 – 900^{o}C near engine (hot section) to 100 – 350^{o}C for parts situated at a distance from engine such as mufflers and tail end pipe (cold section) [1]. The material properties of exhaust required for hot section include high-temperatures strength, thermal fatigue properties, oxidation resistance and salt corrosion resistance. While the same required for cold section away from engine is corrosion resistance to salt damage and exhaust gas condensate. The corrosion problem is mostly observed during-short distance driving, when the temperature does not increase and wet corrosion due to condensation mainly in muffler at cold end becomes the major factor of failure [2]. Typical types of corrosion mechanisms observed in exhaust systems include general corrosion, pitting corrosion, crevice corrosion, inter-granular corrosion, and oxidation, etc. Corrosion failures may cause perforation of components causing exhaust leaks in internal components that may result in noise issues due to change in muffler acoustics and can also result in pollution causing damage to environment. Perforation can be a small area due to localised corrosion such as pitting in which pits can penetrate the material thickness [3].

Pitting corrosion is one of the major problems due to which automotive exhaust components have a limited lifetime as it is basically attacking the muffler since long ago. Even stainless steel does not possess effective corrosion resistance due to very highly aggressive environment. The resistance of different steel grades to pitting corrosion can generally be compared on the basis of their alloy composition via their pitting resistance equivalent number, PREN [4]. However, this is questionable for the special conditions existing in automotive exhaust systems, with their frequent wet/dry alternation and their short operating times compared with overall life cycles [5]. The important area of research is not only on the selection of material for maximum resistance to the onset of pitting corrosion but also on how the pitting can be monitored as well as predicted using the state of art condition monitoring technique. This technique if incorporated in muffler design of modern automotive applications e.g. cars can help to prevent early failures of exhaust systems under wet conditions.

This research focuses mainly inside wet corrosion of automotive exhaust muffler at cold end. Wet corrosion of inner muffler wall due to gas condensation is one of the major causes of muffler failure [5]. The condensation of water droplets and dissolution of corrosive gases in droplets act as a major medium for internal corrosion of muffler incorporating the high contents of carbonate ions, sulphate ions, nitrate ions and chloride ions which constantly accumulate as the engine repeatedly starts and stops [6]. This condensation process produces carbonic acid, sulphuric acid, nitric acid and low levels of hydrochloric acid, creating critical conditions with acidic pH-values which act as an ideal medium for pitting corrosion on standard exhaust steel [7]. Various stainless steel grades which are highly resistant to pitting are used by the manufacturers in muffler design however they are also much more expensive compared to conventional basic steel [8]. It is still difficult to predict the long term behaviour of corrosion resistant stainless steel when subjected to real environment besides their good corrosion prevention properties. For internal muffler corrosion, vast literatures have been available mainly focusing on material selection for designing highly corrosion resistant mufflers [1, 9-15] however, there are grey areas that need to be researched more in terms of developing predictive modelling techniques to address early failure issues of mufflers due to exhaust gas condensation and corrosion. These predictive models can be utilised by the manufacturers to design durable, high strength and corrosion resistant exhaust mufflers.

Previous research has modelled [16-28] general corrosion on metal surface as a result of coating failure. However, the aim of this research is to develop a mechanistic model for exhaust muffler which is able to predict the condensation rate of water droplets as well as species breakdown in droplets and pitting rate including pit depth. Condensation happens when the temperature of muffler does not go up compared to the saturated vapour flowing inside the muffler. The water vapor in the gas phase condenses on the muffler's inner wall in two different ways (i) bottom of the muffler condensation happens when the condensed liquid on side walls of muffler slides to the bottom due to gravity and forms a flood of liquid at muffler's base (ii) top of muffler condensation happens when the liquid droplets nucleate, grow, detach and then fall due to gravity from the top wall of muffler. The dissolution of corrosive gases which are coming from the internal combustion of engine in the droplet can cause severe pitting corrosion. The area of muffler that is most critical and prone to pitting corrosion is the top wall of muffler where condensation in the form of low pH acidic droplets directly takes place.

This paper discuses a detailed experimental study which was conducted by using mufflers as test bed. These mufflers were subjected to different types of exhaust gas condensates (like petrol and diesel) and were tested for different conditions such as wall temperatures, gas temperatures and gas velocities. Corrosion sensors and condensation sensors which were installed on the inner wall of muffler were used to monitor corrosion rates and condensation rates respectively. Based on the observation recorded from experimentation, a holistic model was developed in which the chemistry inside the droplet was computed from the thermodynamic equilibrium at the interface of liquid gas and the electrochemical activity at metal surface related to the corrosion process. In holistic design, a mechanistic corrosion model was combined with the drop wise condensation model to predict internal muffler corrosion due to exhaust gas condensate. Finally, the model was validated by qualitative comparison between experimental and predicted results showing a good agreement between the two.

2. Experimental

2.1. Experimental setup

Three exhaust mufflers: muffler 1, muffler 2 and muffler 3 of similar dimensions and material properties fabricated using stainless steel were used as test samples. Muffler 2, at the start of experiment, was kept in low concentration sodium chloride (NaCl) solution at 20 °C, 0.65 M of NaCl dissolved in 11.1 M deionized water for 48 h while muffler 3 was kept in high concentration NaCl solution at 20 °C, 0.95 M of NaCl dissolved in 11.1 M deionized water for 48 h. Muffler 1 was only subjected to deionised water at 20°C for 48 h. The sample mufflers were then removed and the inner side of mufflers was air dried to allow chloride ions to deposit on mufflers inner wall. The step was performed to simulate and analyse the effect of road salt on the corrosion of mufflers inner wall.

Next, in order to perform the real time measurements of condensation rate and corrosion rate, the mufflers top cap was removed and the inner wall of each muffler was installed with condensation sensor having dimension 45 mm x 20 mm x 0.2 mm and corrosion sensor having dimension 40 mm x 20 mm x 0.1mm as shown in fig. 1 (a). After installation of sensors, mufflers cap was placed back and sealed in order to assure any gas leak during experimentation. It is worth noting that the area on which the sensors were installed was first conditioned to remove chloride ions which could affect the sensors functionality. The condensation sensors [29] are monolithic integrated micro-sensors for monitoring the water droplets contents. The modules consist of a silicon integrated

stray field capacitor including condensation detection area, a temperature sensor as well as a capacity frequency converter. The condensation of water vapour is monitored by the electrical stray fields and is converted into appropriate output signals. The corrosion sensors [30] consists of multiple plates made from the material of interest which form the two electrodes. The electrodes are used in conjunction with a potentiostat for conducting LPR measurements. The use of a relatively large counter electrode minimizes polarization effects at the counter electrode to ensure that a stable reference potential is maintained throughout the experiments. Potential step-sweeps are performed by applying a series of 30 steps over a range of ±10 mV spanning a period of 2.6 s [31].

Both the condensation and corrosion sensors were adhered to the inner wall of all three mufflers with industrial strength epoxy as shown in fig. 1(a). To guarantee the efficient performance of corrosion sensors, the bonding agent (industrial strength epoxy) was placed on the opposite edges of the corrosion sensors so as to adhere the sensors to the muffler stainless steel wall in a manner such that the ambient environment is allowed to rapidly diffuse between the sensors and the steel. In order to allow the vapour condensation inside muffler, the outer wall of muffler was fitted with the condenser in which cooling fluid from cooling tower was circulated through the tubes as shown in fig 1(b). The low temperature of wall, lower than the temperature of gas allows the water droplets to accumulate on the wall surface.

2.2. Accelerated testing and observations

The accelerated condensation corrosion testing for all three mufflers with pre-existing chloride deposits (in muffler 2 and 3) was performed by allowing the exhaust gas to pass through mufflers and at the same time cooling the mufflers walls by circulating the cooling water from cooling tower through the condenser tube. The gas temperature and gas velocity were set as 333 K and 2 m/s respectively and the test ran constantly for 17 successive days (408 hours). The low temperature of wall allowed the nucleation of water droplets on the inner side walls and top walls while surrounding gas flow accelerated the corrosion due to diffusion of corrosive gas species through water droplets. For real time condensation monitoring, the condensation sensors were used to monitor the condensation rate on the inner muffler wall by measuring the water droplets contents in the area surrounding the sensor. The average wall temperature of three mufflers and corresponding condensation rates for each muffler with respect to accelerated testing time is shown in fig. 2. (a) The results show that condensation rate increases with the decrease in wall temperature and then becomes constant with stable low wall temperature.

In order to analyse the effect of corrosive gas species on the corrosion of all mufflers, each muffler was also passed with the exhaust gas of different percentage composition. The exhaust gas composition for each muffler is shown in table 1. Muffler 1 was passed with pure air having no significant traces of any corrosive species, muffler 2 was passed with gas (similar to diesel engine) having some contents of corrosive species such as nitrogen oxides, carbon monoxide, hydrocarbons and sulphur dioxide. Muffler 3 was passed with gas (similar to petrol engine) having considerable large contents of corrosive species. These corrosive species combined with an accumulation of chloride ions diffuse through water droplets on mufflers wall where they dissociate and produce carbonic acid, sulphuric acid, nitric acid and small levels of hydrochloric acid creating critical conditions with acidic pH-values. The condensate from three mufflers was collected to perform pH and chemical trace analysis (CTA). The CTA was performed to evaluate the condensate composition showing that the condensate was composed of chloride ions Cl^-, carbonate ions CO_3^- , sulphate ions $SO_4^{2-}$and nitrate ions NO_3^- as shown in table 2. Results showed that condensate collected from muffler 1 which was passed with pure air had pH close to neutral (~ 6) with no traces of corrosive ions. The condensate from muffler 2 showed pH equal to 4 with some traces of $Cl^-, CO_3^-, SO_4^{2-}$and NO_3^- however, in case of muffler 3, the condensate showed low acidic pH equal to 3 and large traces of Cl^-, $CO_3^-, SO_4^{2-}$and NO_3^-. The acidic pH condensate in case of muffler 2 and 3 resulted in a substantial wet corrosive impact on their inner walls and therefore aggravated pitting corrosion, much intense in muffler 3 and was found absent in muffler 1. For real time pitting corrosion monitoring, the linear polarization resistance measurements were used to compute corrosion pit depth for each muffler. The pit depth $d(t)$, μm corresponding to pit density N_{pit}, cm^{2-} for all the three mufflers due to corrosion as shown in fig. 2 (b) was calculated by using relation [32],

$$\mathbf{d(t) = \sqrt[3]{\frac{3T_{sam}EW}{2\pi\rho N_{pit}F}\int_0^t\left(\frac{B}{A_{sen}R_p(t)} - i_{pv}\right)dt}} \qquad \mathbf{1}$$

Where, N_{pit} was calculated by counting the number of pits over an area of 1 cm^2 on all mufflers surface using microscopy; i_{pv}, A/cm^2 is the passive current density; A_{sen}, cm^2 is the effective surface area of the corrosion sensor; EW, g/mol represents the equivalent weight of the metal that reacts with 1 C of charge, thus contributing to the corrosion and overall loss of material in the anodic (oxidation) reaction; ρ, g/mm^3 is the density of steel;

R_p, Ω is the polarization resistance between the corrosive agents (electrolytic droplets) and the steel substrate which in practice is not measured continuously by sensor, rather, periodic measurements are taken every T_{sam} seconds; B, V/dec is called Stern-Geary constant having value of 30 mV for carbon steel [33]; F is the faradays constant. All the three mufflers were analysed using scanning electron microspore (SEM). The results showed highest pitting density in muffler 3, moderate in muffler 2 and least in muffler 1 as show in fig. 3.

To ensure repeatability, the experiment was repeated by considering two cases. Case 1: changing gas temperature from 333 K to 313 K and keeping constant gas velocity 2 m/s; Case 2: keeping constant gas temperature 333 K and changing gas velocity from 2 m/s to 15 m/s. For case 1, the results showed that low gas temperature (313 K) compared to previous high gas temperature (333 K) resulted in high condensation because of near saturation conditions of vapours. The high condensation rate resulted in more fresh water available to drive large pitting corrosion rate (pit depth) in the mufflers as shown in fig. 4 (a-b). For case 2, the condensation rate for all the three mufflers was found to be high and pitting corrosion rate was found to be almost same in case of high gas velocity 15 m/s compared to low gas velocity 2 m/s as shown in fig. 5 (a-b). The reason is that the high gas velocity turns the static droplet in to sliding and therefore results in large number of droplets distribution over a surface area of muffler's walls however; the overall maximum size of droplets reduces. As the static droplets now turn in to sliding therefore more and more surface of muffler's internal wall become covered with Fe_3S_4, Fe_3C leading to overall increase of the space-averaged corrosion rate. However, the corrected localised corrosion rate in terms of pit depth is not much affected by gas velocity as shown in fig. 5 (a-b).

Based on observation from above experimentation, a holistic model incorporating the concepts of both condensation and corrosion has been developed in the next section.

3. Mathematical model

3.1. Condensation model

The problem of condensation mainly persists during short distance runs of vehicles, when the temperature does not increase and the condensation occurs particularly inside the muffler component closest to the tail pipes [2]. At the start, a discontinuous film of liquid can form on the metal surface due to the drop wise condensation of liquid. The drop wise condensation is a type of mixed-form condensation process, in which small liquid droplets grow at the interface between a stable saturated vapor and another solid phase. These tiny droplets increase in size with the continuous condensation of vapor on the gas-liquid interface. The droplets combine with the neighbouring droplets due to continuous increase in droplet size. Thus, the water droplet size increases either due to conjoining with nearby droplets or due to on-going vapor condensation. The increased size droplet, as a result of drag force due to high velocity from the surrounding gas flow results in the movement of droplet in the direction of gas flow. This process results in the continuous sweeping of any adjacent droplets in its way ahead.

When an individual droplet acquires its maximum size, the droplet may drift down along the inner surface of the exhaust wall due to the gravity pull. Both forward and downward movements can be observed in this case. For the case when the surrounding gas flow is slow, the droplets may detach from the top of exhaust wall and fall to the bottom providing with vacant space for the development of new droplets. The process of development, moving forward and falling will repeat again as a new cycle. The development of droplets due to condensation is a random process; therefore an analytical method is deployed to model the droplet size distribution and overall heat transfer process. The calculated values of ***droplet size distribution*** and the ***total heat flux*** through the droplets are then utilised for calculating the condensation rate for drop wise condensation.

The inner surface of exhaust at a given time during short distance runs is occupied with droplets of different random radii, which is called as ***droplet size distribution***. The Rose equation can be utilised as a droplet size distribution function [34],

$$\mathbf{N(r)dr} = \frac{\mathbf{n}}{\pi \mathbf{r}^2 \mathbf{r_{max}}} \left(\frac{\mathbf{r}}{\mathbf{r_{max}}}\right)^{\mathbf{n-1}} \mathbf{dr} \qquad \mathbf{2}$$

Where, $N(r)dr$ is the number of droplets having radius r over surface area of 1 m^2; n =1/3 is the exponent constant; r_{max} is the maximum droplet radius in m [35].

$$\mathbf{r_{max}} = \sqrt{\frac{\mathbf{K'}}{\rho \mathbf{H_{fg}}}} \quad 1$$

Where, ρ is the water density, kg/m^3; H_{fg} is the latent heat of evaporation/condensation for water, J/kg; K′ is the resultant force on droplet which depends on the properties of gas and on the conditions (e.g. roughness) of exhaust wall surface.

$$\mathbf{K'} = \sqrt{(\mathbf{F_f^x} - \mathbf{F_D^x})^2 + \left(\mathbf{F_\sigma^y} + \mathbf{F_B^y} - \mathbf{F_g^y} - \mathbf{F_D^y}\right)^2} \quad \mathbf{4}$$

Where, F_f^x represents the bonding between droplet and the steel wall which acts as an opposition to the drag force and allows the droplet to stay in place; F_D^x represents the drag force exerted on the droplet by the flowing gas; F_σ^y represents the surface tension and allows the droplet to remain attach to the exhaust wall and counters the effect of gravity; F_B^y represents the buoyancy for a suspended semi-circular droplet; F_g^y represents the gravity force which tends to either detach the droplet from the top of the exhaust or cause it to slide down the sides of the exhaust; F_D^y represents the downward drag force which rises due to the semi-circular shape of the droplets. All these forces, for an individual droplet are represented in fig. 6.

$$F_f^x = k_f \sigma r \quad 4(a)$$

$$F_D^x = \frac{C_D \rho_g r^2 \pi v_g^2}{4} \quad 4(b)$$

$$F_\sigma^y = \pi r^2 \left(\frac{2\sigma}{r}\right) \quad 4(c)$$

$$F_B^y = 0.7 \pi r^3 \rho_g \quad 4(d)$$

$$F_g^y = 0.7 \rho \pi r^3 g \quad 4(e)$$

$$F_D^y = \frac{F_D^x}{2} \quad 4(f)$$

Where, k_f is the coefficient of friction which is a function of inner exhaust surface roughness h such that when h < 0.5 μm and becomes constant when h > 0.5 μm [36]; σ is the vapor-liquid surface tension, N/m; C_D is the drag coefficient; v_g is the velocity of gas, m/s; ρ_g is the gas density, kg/m^3; g is acceleration of gravity, 9.81 m/s^2.

The ***total heat flux Q***, W/m^2 for a unit area of the exhaust wall (1 m^2) covered by a vast number of droplets $N(r)$ of numerous radii (sizes) can be evaluated by summation of the heat fluxes q(r) for droplets from minimum radius to maximum radius, which can be written as [37],

$$\mathbf{Q} = \int_{\mathbf{r_{min}}}^{\mathbf{r_{max}}} \mathbf{q(r)N(r)dr} \quad \mathbf{5}$$

Where r_{min} is the minimum radius of droplet, m in a unit area; $q(r)$ is the amount of heat transferred through a droplet of radius r [38].

$$r_{min} = \frac{2T_s\sigma}{H_{fg}\rho\Delta T} \quad 5(a)$$

$$\mathbf{q(r)} = \frac{\mathbf{T_i^g}\left(1 - \frac{2\sigma}{\mathbf{H_{fg}} r \sigma}\right) - \mathbf{T_o^w}}{\frac{\mathbf{r}}{4\pi \mathbf{r^2 k_{H_2O}}} + \frac{1}{2\pi \mathbf{r^2 h_i}} + \frac{\mathbf{d_w}}{4\pi \mathbf{r^2 k_w}}} \quad 5(b)$$

Where, T_s is the saturation temperature; ΔT is the difference of saturation temperature between curved surface and flat surface of the gas-liquid interface (sub cooling temperature) which is supposed as the minimum driving force to form a droplet on the solid surface; T_i^g is the temperature at the surface of droplet; T_o^w is the temperature at the outer exhaust wall; k_{H_2O} is the thermal conductivity of water, W/m/K; k_w is the thermal conductivity of the exhaust wall, W/m/K; h_i is the heat transfer coefficient at the droplet interface, W/m^2 /K; d_w is the thickness of exhaust wall, m. All the temperature coefficients and temperature gradient is shown in fig. 6.

The total heat flux Q, temperature at the surface of droplet T_i^g, temperature of the bulk gas T_b^g and heat transfer coefficient for the gas boundary layer h_g, W/m^{2}K can be used to calculate the condensation rate $\dot{m}$, kg$_g$/m^2/s as,

$$\dot{m} = \frac{Q - h_g(T_b^g - T_i^g)}{H_{fg}} \quad 6$$

The heat transfer coefficient h_g can be related with the mass transfer coefficient β_g , m/s^2 for the gas boundary layer as [39],

$$h_g = \frac{\rho_g \beta_g \widehat{C_p}}{Le^{\frac{2}{3}}} \quad 7$$

$$Le = \frac{k_g}{\rho_g \widehat{C_p} D_v} \quad 7(a)$$

Where, k_g represent the thermal conductivity of gas, W/m·K. In presence of non-condensable gases, the resistance to mass transfer of water vapor in the boundary layer can be rather very high. This makes the coupling relation of heat and mass transfer and therefore they need to be solved simultaneously.

The size of droplet gradually increases due to condensation; this is simulated as a two dimensional problem in order to avoid mathematical complications. When the size of the droplet reaches a maximum height, the droplet detaches from the surface and a new droplet nucleates at its place; this is simulated by again setting the droplet size from r_{max} to r_{min} representing the start of new cycle again.

3.2. Corrosion model

Pitting corrosion of automotive exhaust (or anywhere) is a multi-process phenomenon involving two simultaneous processes (i) ***transport of species*** in the water droplet (ii) ***hydrolysis and electrochemical reaction***s in pits resulting in pit growth. The corrosion model utilises the constants in the equation system taken from the open literature referenced by Walton's papers [40]. These constants include equilibrium constants, reaction rate constants and diffusion coefficients.

The expression for the ***transport of species*** *through the liquid droplet* in the presence of chemical reactions follows Fick's species conservation equation [41]

$$\frac{\partial \varepsilon c_i}{\partial t} = -\frac{\partial}{\partial y}\varepsilon^{1.5}(\underbrace{-z_i D_i c_i \nabla\phi}_{\text{Migration}} - \underbrace{D_i \nabla c_i}_{\text{Diffusion}}) + \underbrace{c_i v}_{\text{Convection}} + R_i \quad 8$$

Where, the term on the left-hand side represents the rate of change of concentration with time t (accumulation) and on the right-hand side the term D_i represent the diffusion coefficient of species i, m^2/s; ϕ represents the droplet liquid potential; z_i is the charge number for species i; Furbeth et al [42-44] reported that the permeability of porous medium (such as scale) for transport of species can be written as $\varepsilon^{1.5}$ where, ε represents the situation where the corrosion cavity is partially filled with gas or solid phase corrosion products such as hydrogen gas, metal oxides or salts. The liquid porosity is the proportion of the cavity volume which is filled with the liquid phase. When corrosion products are not present in the cavity, the porosity is equal to one [40]; v is the local velocity of liquid in the droplets; R_i is the total rate of reaction of species 'i' in solution (moles m^{-3} s^{-1}).

The terms on the right-hand side of eq. 8 represent, respectively, migration, diffusion and convection contributions to the flux. It is assumed, at first that the liquid in the droplets is stationary, and therefore no convection term exists in the species conservation equation i.e. v = 0. Secondly, the migration is neglected as well, and the electro neutrality equation is used instead i.e. $\sum_i z_i . c_i = 0$. By considering the above assumptions and substituting in eq. 8, the overall species conservation equation in the droplet containing only diffusion term can be expressed as,

$$\frac{\partial \varepsilon c_i}{\partial t} = D_i \frac{\partial^2}{\partial y^2}(\varepsilon^{1.5} c_i) + R_i \quad 9$$

The corroding media responsible for internal exhaust corrosion is a gas condensate, with high SO_4^{2-} and CO_3^{-} content. The diffusion of these species results in the formation of pits on internal walls of exhaust. Two types of chemical reactions are of interest in pits: (i) reactions in the pit solution (e.g. ***hydrolysis)***, and (ii) electrochemical reactions at the metal-solution interface.

An example of *hydrolysis reaction* involves the hydrolysis of iron which can be written in the form of kinetic expressions (e.g. 1st order kinetics) as,

$$Fe^{2+} + H_2O \longleftrightarrow Fe(OH)^{+} + H^{+}$$

It is assumed that the reaction in solution remains in equilibrium state and therefore kinetic equilibrium expression can be used to express the reaction rate of species inside the pit solutions. One method for modelling the equilibrium state in solution is to keep the governing equations in rate format but make the reaction rates very fast. As long as reaction rates are fast, relative to rates of mass transport in water droplet, the reactions will remain at equilibrium and the solution is independent of the kinetics assumed. In this research, the following rate reaction expression, obtained from transition state theory for reactions near equilibrium, is used [40],

$$\mathbf{R_i} = \sum_{\mathbf{k=1}}^{\mathbf{k_{max}}} \left[-\mathbf{r_k}\, \mathbf{v_{ik}} \ln \left[\frac{\prod_{\mathbf{i=1}}^{\mathbf{i_{max}}} \mathbf{c_i^{v_{ik}}}}{\mathbf{K_k}} \right] \right] \qquad \mathbf{10}$$

Where, r_k is the adjustable numerical rate parameter for reaction k (moles m^{-3} s^{-1}) and K_k is the equilibrium constant for reaction k.

Examples of *electrochemical reactions* at the metal-solution interface are the hydrogen evolution (cathodic) reaction and dissolution of the metal (anodic). A number of electrochemical reactions j at the metal surface take place as,

Cathodic reactions:

Hydrogen reduction $\quad 2H^{+} + 2e^{-} \rightarrow H_2$

Water reduction $\quad 2H_2O + 2e^{-} \rightarrow H_2 + 2OH^{-}$

Anodic reactions:

Electrochemical dissolution of iron $\quad Fe \rightarrow Fe^{2+} + 2e^{-}$

As a simplifying assumption, concentrations of species 'i' in the water droplet are assumed uniform in the cross-width directions. This assumption will be valid when the length of the pit cavity is significantly greater than the width (i.e. relatively deep pits). The governing transport equation for a deep cylindrical pit is derived by modifying eq. 9 as,

$$\frac{\partial \varepsilon \mathbf{c_i}}{\partial \mathbf{t}} = \boldsymbol{D_i} \frac{\partial^2}{\partial \mathbf{y^2}} \left(\boldsymbol{\varepsilon^{1.5} c_i} \right) + \frac{\mathbf{2N_i}}{\boldsymbol{\varepsilon^{1.5}} \mathbf{r}} + \mathbf{R_i} \qquad \mathbf{11}$$

Where r is the radius of pit, m; N_i, moles $m^{2-}s^{1-}$ is the rate of chemical reaction/mass transfer for each aqueous species at the metal-solution interface which is obtained from the current density of the electrochemical reactions using Faraday's law as,

$$N_i = \sum_{j=1}^{j_{max}} \frac{v_{ij} i_{pit}}{n_j F} \qquad 11(a)$$

$$i_{pit} = f(\phi_{Fe^{2+}} - \phi, c_1, c_2, \ldots\ldots, c_n) \qquad 11(b)$$

Where v_{ij} is the stoichiometric coefficient of species 'i' in reaction j and n_j is the stoichiometric coefficient of electrons in reaction; i_{pit} , A/m^2 is the pitting current density resulting from an electrochemical reaction at the metal solution interface and is generally expressed as a function of the corrosion potential and the concentrations of some aqueous species (e.g. Butler-Volmer kinetics); $\phi_{Fe^{2+}}$ is the potential of metal (volt). By using pitting current density i_{pit}, it is possible to calculate pit depth as,

$$d(t) = \sqrt[3]{\frac{3EW}{2\pi\rho N_{pit} F}\int_{t_i}^{t_f}(i_{pit} - i_{pv})dt} \quad (12)$$

Where, t_i is the time to initiate the pit; t_f represents the total time over which i_{pit} is calculated.

4. Model solution and validation

The nonlinearly coupled equations are solved simultaneously using finite difference method (FDM), together with the boundary conditions and initial conditions. The species conservation and pitting current density equations are discretized using a FDM. For a stable equilibrium solution of differential equations, an implicit time discretization scheme is employed herein, and all nonlinear terms are linearized in variable space.

Although most of the equations described for the corrosion model are based on conventional methods however, the domain of calculation had to be adapted to the mufflers corrosion scenario in order to take into account the pitting and growth of water droplets with time.

In order to simulate the growth of water droplet due to condensation, the outer boundary of droplet is controlled by varying the position of liquid-vapour interface. When the droplet first nucleates with minimum radius at the muffler wall, the initial concentrations of corrosive species are set equilibria for clean freshly condensed water. With the increasing radius of the droplet, the outer boundary of the computational domain is also enlarged however upon reaching sufficient large size, the droplet detaches from the wall and the computational domain minimises back to initial nucleation size. This domain minimisation does not alter the concentration of corrosion species which remain same as before droplet detachment. The muffler mainly faces pitting corrosion, however if the corrosion results in the formation of scales along with pitting, than the new droplet will nucleate on the outside of exiting corrosion scale. In this case, the computational domain will have thickness equal to scale thickness plus the new droplet size.

4.1. Condensation model validation

The condensation model can be employed to predict the condensation rate for various regimes of water droplets under different environmental conditions. The model is validated by making some quantitative comparisons between the experiments and the theoretical discussion of the previous sections. It was emphasised in experimental section 2 that the *wall temperature* has a profound influence on the condensation rate specific to constant conditions: T_b^g = 333 K, v_g = 2 m/s. The comparison between experiment and model prediction of condensation rate for decreasing wall temperature with respect to time is shown in fig. 7 (a). The mean of experimental condensation rates for all three mufflers were compared with the simulated results from condensation model. The model gave a good prediction of condensation rate with respect to changing wall temperature. In a separate series of experiments, the effect of *gas temperature* on condensation rate was analysed by now setting the low gas temperature T_b^g = 313 K compared to high T_b^g = 333 K which was set previously in fig. 7 (a). For newly set low gas temperature T_b^g = 313 K, the condensation rate was found to be much higher because of near saturation conditions of vapours. This condition was simulated using model showing a good agreement between predications and experimental results as shown in fig. 8 (a). Another set of experiments was performed to analyse the effect of *gas velocity* on condensation rate by now setting high gas velocity v_g = 15 m/s compared to low gas velocity v_g = 2 m/s which was set previously. The results showed the large condensation rate for high gas velocity due to gas drag force. The reason for high condensation rate with increased gas velocity is mainly the spread of larger number of droplets over a surface area of meter square however; the overall maximum size of droplets reduces. This condition was simulated and compared with experimental curves showing a good agreement between the two as shown in fig. 9 (a).

4.2. Corrosion model validation

In most of muffler corrosion cases, the general pit depth is expected to increase linearly since the chemistry in the fresh condensed droplets is ideal for the formation of low acidic pH condensate due SO_4^{2-}, CO_3^- and Cl^- ions diffusion in droplets. These species result in the formation of low pH electrolyte on metal surface and therefore aggravating the pitting. From Figure 7 (b) which shows a typical simulation result for *wall temperature* values specific to constant conditions: T_b^g = 333 K, v_g = 2 m/s, it can be seen that the pit depth increases linearly with the passing time (hours). The 'stair-case' appearance of the pitting depth is due to the many droplets that form,

[illegible] or step [illegible] droplets lifetime. Clearly when new freshly condensed droplets form, the pitting depth increases dramatically shown by vertical step in each stair-case and then slowly shown by horizontal as droplets saturate with $FeSO_4, FeCO_3$ and $FeCl_3$, leading to a slight pH increase. In the simulation, it was found that in the electrolyte droplet surrounding the pit, both the concentration of Fe ions and pH become slightly higher with time compared to freshly condensed droplet with low pH. For example at these conditions (Fig. 7 (b)) in case of muffler 3, the pH in fresh condensed water is 3, which is also the boundary condition at the interface of the droplets. But at the metal surface and inside the pit, the Fe ion concentration builds up due to corrosion reaction. Due to the corrosion process the pH increases dramatically and reaches up to 4.5, which leads in stable slow growth of pit's depth. [illegible] simulated results in fig. 7 (b) showed a good agreement with the experimental results.

In a separate series of experiments, from fig. 8 (b), it follows that for a low *gas temperature* when T_b^g was set at low 313 K compared to previous high 333 K (in fig. 7 (b)), the resultant pit depth was observed to increase. Low gas temperature accounts for higher condensation rate which results in increased pit depth. The reason for this is probably that there is more fresh water available at higher condensation rate. Moreover, the saturation of $FeSO_4, FeCO_3$ and $FeCl_3$ is easier to achieve when there is less water (at lower condensation rate, the droplet grows slower and is refreshed in less frequency). Both the experimental and simulation results for the above conditions in fig. 8 (b) were in good agreement.

For another set of data shown in fig. 9 (b), the most visible influence of *gas velocity* on condensation regime can be observed. It was found that by keeping constant gas temperature (e.g. T_b^g = 333 K), high gas velocity v_g= 15 m/s compared to low gas velocity v_g= 2 m/s accounts for large condensation rate however no significant change in pitting rate (in terms of pit depth) is observed. At low velocity (e.g. 2 m/s), the vapour condenses by forming stagnant droplets at the top wall of muffler. In these stagnant droplets, the pitting corrosion takes place in accordance with the life-circle of water droplet i.e. droplets nucleate, grow and detach. However, for high gas velocity (e.g. 15 m/s) the gas drag force increases which results in the transition of condensation regime from stagnant to sliding droplet. It is worth nothing that the trend lines in fig. 9 (b[illegible]cause in sliding case, the droplets slide along the top wall of the mufflers due to gas drag force instead of falling due to gravity; therefore, the nucleation, growth and detachment cycle in form of '[illegible]' now becomes straight line for high gas velocity. For the case of corrosion rate, it was observed that at high gas velocity (15 m/s), [illegible] due to sliding behaviour of droplets become covered with Fe_3S_4, Fe_3C leading to overall increase in the space-averaged corrosion rate. However, the corrected corrosion rate in terms of localised pit depth does not seem to be much affected by gas velocity. The comparison between fig. 9(b) of high gas velocity (15 m/s) with fig. 7(b) of low gas velocity does not show a significant difference in corrosion rate in terms of pit depth.

5. Conclusion

A predictive model for life assessment of automotive exhaust mufflers has been developed, which combines following processes: drop wise condensation, liquid/gas equilibria and corrosion activity at metal surface. An initial calculation developed the mechanics for the growth of water droplets and the chemistry inside the droplet based on thermodynamic equilibrium at the liquid/gas interface. A second calculation produced the electrochemical reaction kinetics at the steel surface and by taking into account the corrosive species transport and corrosion reactions occurring inside the droplet. The model takes into account the most important parameters in corrosion of muffler: wall temperature, combustion gas temperature and combustion gas velocity. All the effects are described as mathematical equations which are strongly based on phenomena involved. The model is able to predict the dropwise condensation rate and pit depth with respect to time.

A model experiment, using various conditions was performed in conjunction with the analysis. The experiment showed good qualitative agreement with the trends predicted by theory.

Acknowledgements

This research is joint funded by Defence Science and Technology Laboratory (DSTL), Ministry of Defence (MoD) and Bournemouth University UK. The authors acknowledge their support and contributions.

References

[1] Y. Inoue and M. Kikuchi, "Present and future trends of stainless steel for automotive exhaust system," *High-temperature,* vol. 950, p. 750, 2003.

[2] J. A. Douthett, "Designing stainless exhaust systems," *Automotive Engineering,* vol. 103, 1995.

[3] Z. Wei, T. Goehring, M. Mioduszewski, L. Luo, A. Kotrba, M. Rybarz*, et al.*, "Chapter 18 - Failure mechanisms and modes analysis of vehicle exhaust components and systems," in *Handbook of Materials Failure Analysis with Case Studies from the Aerospace and Automotive Industries*, A. S. H. M. Aliofkhazraei, Ed., ed Boston: Butterworth-Heinemann, 2016, pp. 393-432.

[4] H. Grafen, "Pitting corrosion of stainless steels," *Materials and Corrosion,* vol. 47, pp. 16-26, 1996.

[5] C. Hoffmann and P. Gümpel, "Pitting corrosion in the wet section of the automotive exhaust systems," *J. Achiev. Mater. Manuf. Eng,* vol. 34, pp. 115-121, 2009.

[6] M. L. Doche, J. Y. Hihn, A. Mandroyan, C. Maurice, O. Hervieux, and X. Roizard, "A novel accelerated corrosion test for exhaust systems by means of power ultrasound," *Corrosion Science,* vol. 48, pp. 4080-4093, 12// 2006.

[7] T. Ujiro, M. Kitazawa, and F. Togashi, "Materials selection and design," ed: December, 1994.

[8] A. Handbook, "Materials selection and design," *Ed. Dieter, EG ASM, Materials Park, OI-I,* vol. 998, 1997.

[9] T. Ujiro, M. Kitazawa, and F. Togashi, "Corrosion of muffler materials in automotive exhaust gas condensates," *Materials Performance;(United States),* vol. 33, 1994.

[10] E. Sato and T. Tanoue, "Present and future trends of materials for automotive exhaust system," *Nippon Steel Technical Report,* vol. 64, 1995.

[11] M. R. Reddy and D. K. M. Reddy, "Design And Optimization Of Exhaust Muffler In Automobiles," *International Journal of Engineering Research and Applications,* vol. 2, pp. 395-398, 2012.

[12] M. Doche, J. Hihn, A. Mandroyan, C. Maurice, O. Hervieux, and X. Roizard, "A novel accelerated corrosion test for exhaust systems by means of power ultrasound," *Corrosion science,* vol. 48, pp. 4080-4093, 2006.

[13] A. Miyazaki, J. Hirasawa, and S. Satoh, "Advanced stainless steels for stricter regulations of automotive exhaust gas," *Kawasaki Steel Tech Rep,* pp. 21-28, 2000.

[14] D. Potente, "General design principles for an automotive muffler," in *Proceedings of ACOUSTICS*, 2005, pp. 153-158.

[15] C. Chen, C. J. Shang, J. Weng, and D. Y. Li, "Corrosion behavior of a new developed ferritic stainless steels used in automobile exhaust system," in *Advanced Materials Research*, 2010, pp. 102-106.

[16] A. Saeed, Z. Khan, M. Clark, M. Nel, and R. Smith, "Non-destructive material characterisation and material loss evaluation in large historic military vehicles," *Insight-Non-Destructive Testing and Condition Monitoring,* vol. 53, pp. 382-386, 2011.

[17] A. Saeed, Z. A. Khan, M. Hadfield, and S. Davies, "Material Characterization and Real-Time Wear Evaluation of Pistons and Cylinder Liners of the Tiger 131 Military Tank," *Tribology Transactions,* vol. 56, pp. 637-644, 2013.

[18] A. Saeed, Z. A. Khan, and E. Montgomery, "Corrosion Damage Analysis and Material Characterization of Sherman and Centaur-The Historic Military Tanks," *Materials Performance and Characterization,* vol. 2, pp. 1-16, 2013.

[19] Z. A. Khan, P. Pashaei, R. S. Bajwa, M. H. Nazir, and M. Camak, "Fabrication and characterisation of electrodeposited and magnetron sputtered thin films," *International Journal of Computational Methods & Experimental Measurements (WIT Press),* vol. [In Press], 2015.

[20] M. H. Nazir, Z. Khan, and K. Stokes, "Modelling of metal-coating delamination incorporating variable environmental parameters," *Journal of Adhesion Science and Technology,* vol. 29, pp. 392-423, 2014.

[21] M. H. Nazir, Z. A. Khan, and K. Stokes, "Optimisation of Interface Roughness and Coating Thickness to Maximise Coating-Substrate Adhesion - A Failure Prediction and Reliability Assessment Modelling," *Journal of Adhesion Science and Technology,* vol. 29, pp. 1415-1445, 2015.

[22] M. H. Nazir, Z. A. Khan, and K. Stokes, "A Holistic Mathematical Modelling and Simulation for Cathodic Delamination Mechanism - A Novel and an Efficient Approach," *Journal of Adhesion Science and Technology,* vol. [In Press], 2015.

[23] M. H. Nazir, Z. A. Khan, and K. Stokes, "A unified mathematical modelling and simulation for cathodic blistering mechanism incorporating diffusion and fracture mechanics concepts," *Journal of Adhesion Science and Technology,* vol. 29, pp. 1200-1228, 2015.

[24] M. H. Nazir, Z. A. Khan, and K. Stokes, "Maximising the interfacial toughness of thin coatings and substrate through optimisation of defined parameters," *International Journal of Computational Methods & Experimental Measurements (WIT Press),* vol. [In Press], 2015.

[25] Z. A. Khan, M. Grover, and M. H. Nazir, "The Implications of Wet and Dry Turning on the Surface Quality of EN8 Steel," in *Transactions on Engineering Technologies*, ed: Springer, 2015, pp. 413-423.
[26] M. H. Nazir, Z. A. Khan, A. Saeed, and K. Stokes, "Modelling the Effect of Residual and Diffusion induced Stresses on Corrosion at the Interface of Coating and Substrate," *CORROSION, NACE [Submitted after revisions],* 2015.
[27] M. H. Nazir, Z. A. Khan, A. Saeed, and K. Stokes, "A model for cathodic blister growth in coating degradation using mesomechanics approach "*Materials and Corrosion WILEY [In Press],* 2015.
[28] M. H. Nazir, Z. A. Khan, A. Saeed, and K. Stokes, "The propagation and axisymmetric stability of circular, defect driven coating delamination under the influence of compression and diffusion induced stress," *Engineering Fracture Mechanics, Elsevier [Submitted],* 2015.
[29] "Condensation sensors," http://www.cismst.org/en/loesungen/kondensationssensoren/.
[30] D. W. Brown, R. J. Connolly, D. R. Darr, and B. Laskowski, "Linear Polarization Resistance Sensor Using the Structure as a Working Electrode," *PHM Society, EUROPEAN CONFERENCE OF THE PROGNOSTICS AND HEALTH MANAGEMENT SOCIETY 2014,* vol. 5, pp. 1-7, 2014.
[31] D. Brown, D. Darr, J. Morse, and B. Laskowski, "Theoretical and Experimental Evaluation of a Real-Time Corrosion Monitoring System for Measuring Pitting in Aircraft Structures," *First European Conference of the Prognostics and Health Management Society 2012,* vol. 3, pp. 1-9, 2012.
[32] D. Brown, D. Darr, J. Morse, and B. Laskowski, "Real-time corrosion monitoring of aircraft structures with prognostic applications," in *Annual conference of the Prognostics and Health Management Society*, 2012, pp. 1-12.
[33] D. R. Lide, *CRC handbook of chemistry and physics*: CRC press, Boca Raton, USA, 2004.
[34] J. Rose and L. Glicksman, "Dropwise condensation—the distribution of drop sizes," *International journal of heat and mass transfer,* vol. 16, pp. 411-425, 1973.
[35] M. Mei, B. Yu, J. Cai, and L. Luo, "A fractal analysis of dropwise condensation heat transfer," *International Journal of Heat and Mass Transfer,* vol. 52, pp. 4823-4828, 2009.
[36] J. J. Bikerman, *Physical surfaces* vol. 20: Elsevier, 2012.
[37] J. Rose, "Some aspects of condensation heat transfer theory," *International communications in heat and mass transfer,* vol. 15, pp. 449-473, 1988.
[38] C. Graham and P. Griffith, "Drop size distributions and heat transfer in dropwise condensation," *International Journal of Heat and Mass Transfer,* vol. 16, pp. 337-346, 1973.
[39] K. Stephan and C. V. Green, *Heat transfer in condensation and boiling*: Springer, 1992.
[40] J. C. Walton, "Mathematical modeling of mass transport and chemical reaction in crevice and pitting corrosion," *Corrosion Science,* vol. 30, pp. 915-928, 1990.
[41] K. N. Allahar, M. E. Orazem, and K. Ogle, "Mathematical model for cathodic delamination using a porosity–pH relationship," *Corrosion Science,* vol. 49, pp. 3638-3658, 2007.
[42] W. Fürbeth and M. Stratmann, "The delamination of polymeric coatings from electrogalvanised steel–a mechanistic approach.: Part 1: delamination from a defect with intact zinc layer," *Corrosion science,* vol. 43, pp. 207-227, 2001.
[43] W. Fürbeth and M. Stratmann, "The delamination of polymeric coatings from electrogalvanized steel–a mechanistic approach.: Part 2: delamination from a defect down to steel," *Corrosion science,* vol. 43, pp. 229-241, 2001.
[44] W. Fürbeth and M. Stratmann, "The delamination of polymeric coatings from electrogalvanized steel–a mechanistic approach.: Part 3: delamination kinetics and influence of CO2," *Corrosion science,* vol. 43, pp. 243-254, 2001.

Figure

Figures

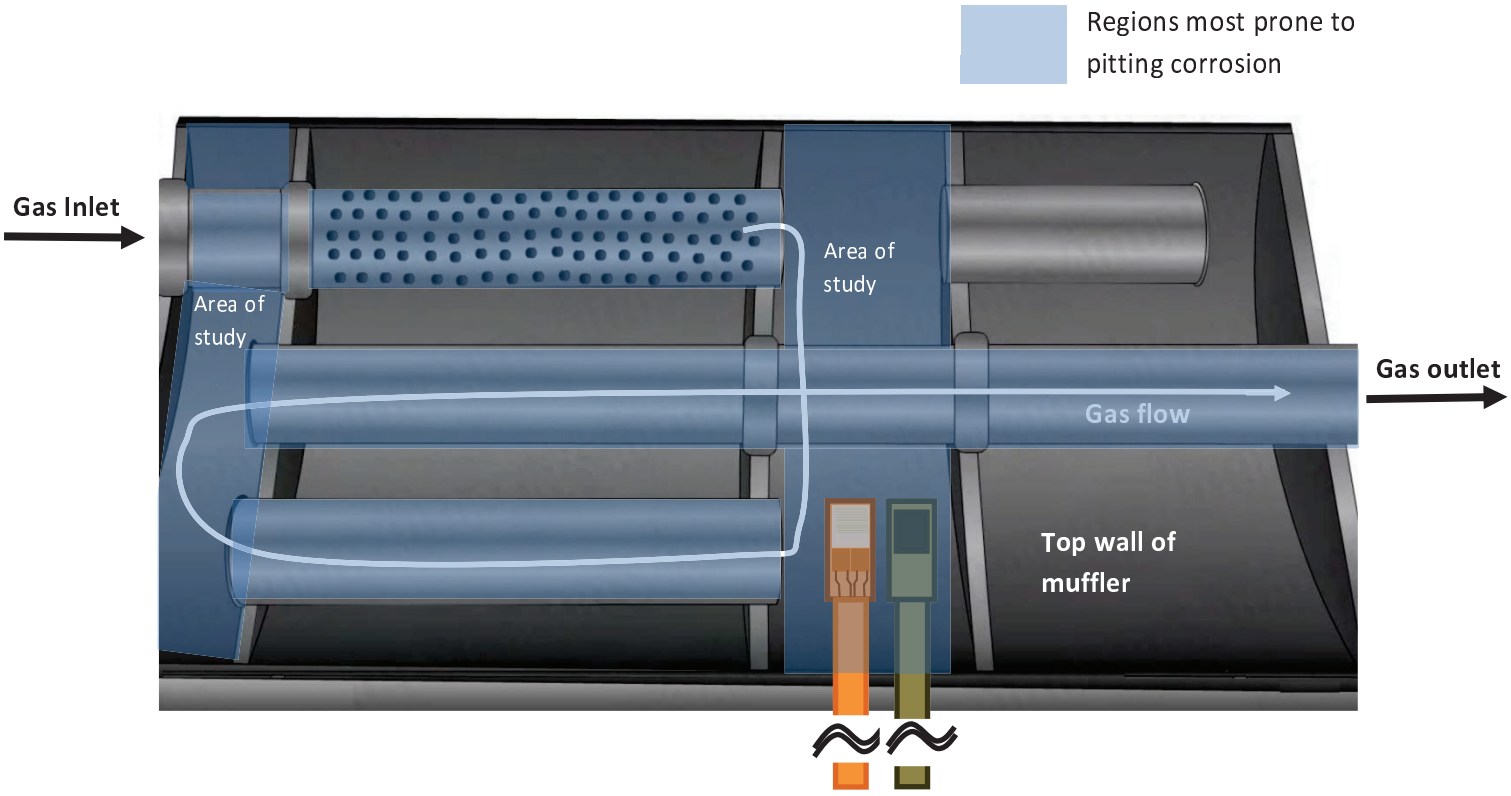

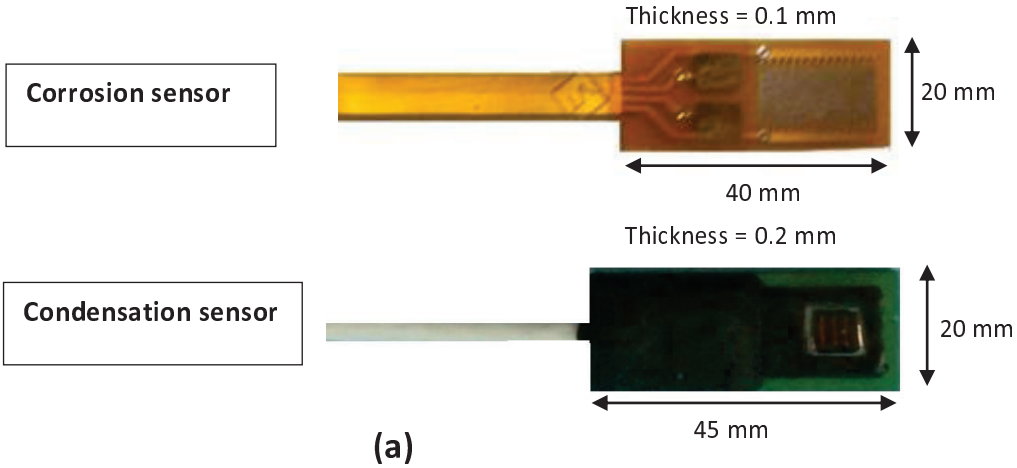

(a)

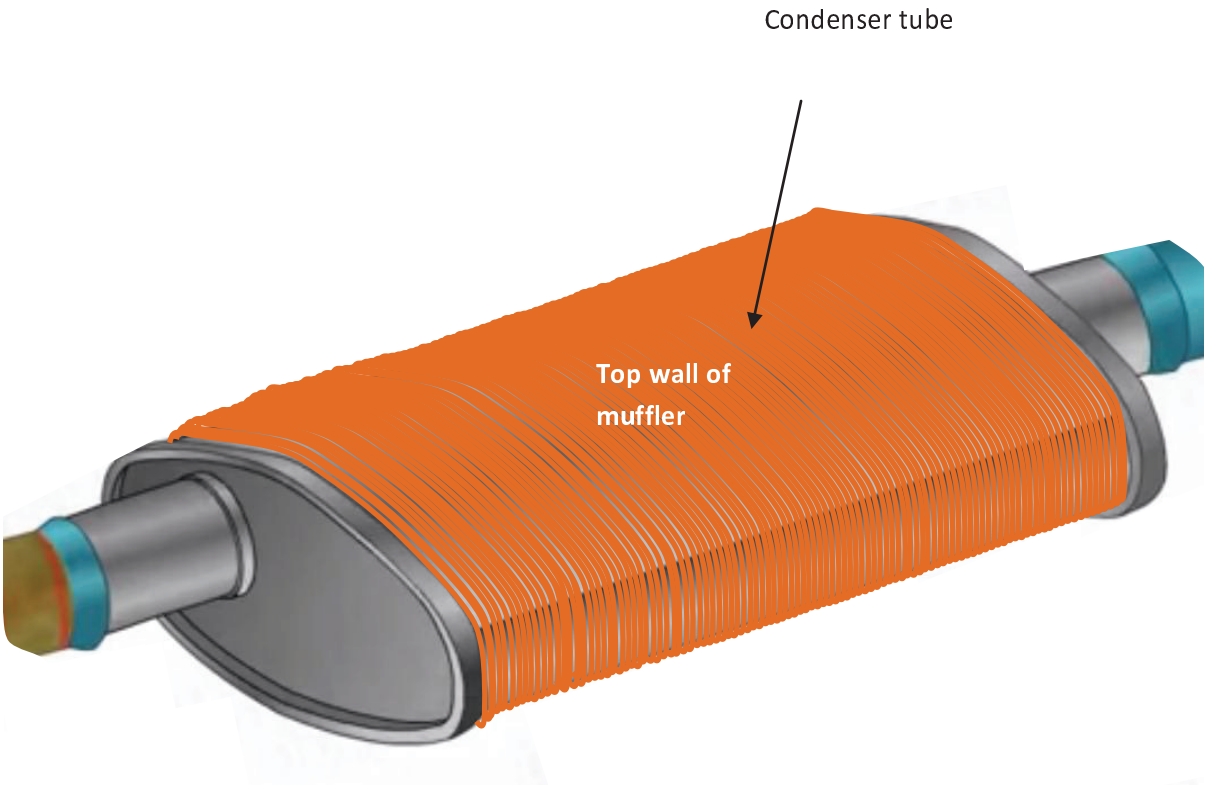

Figure 1. (a) Automotive exhaust muffler, corrosion sensors and condensation sensor (b) Outer wall of muffler fitted with the condenser in which cooling fluid from cooling tower is circulated through the tubes.

(a)

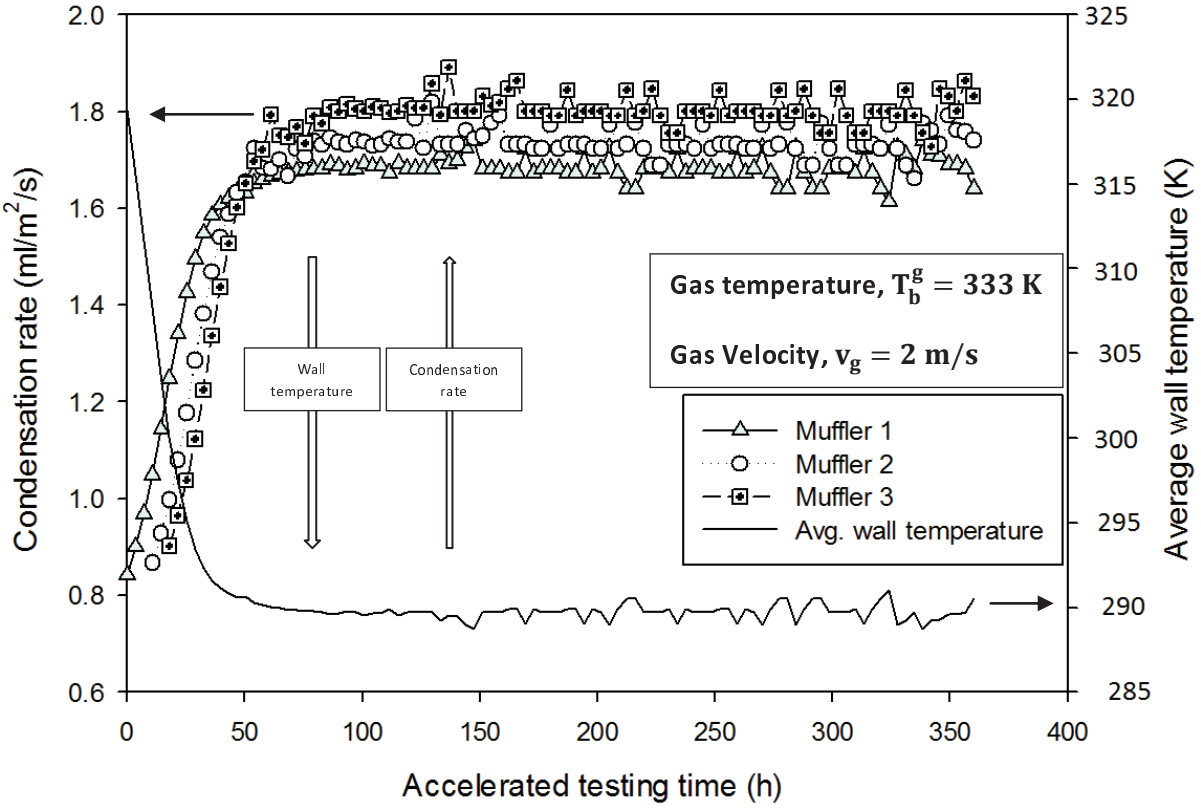

(b)

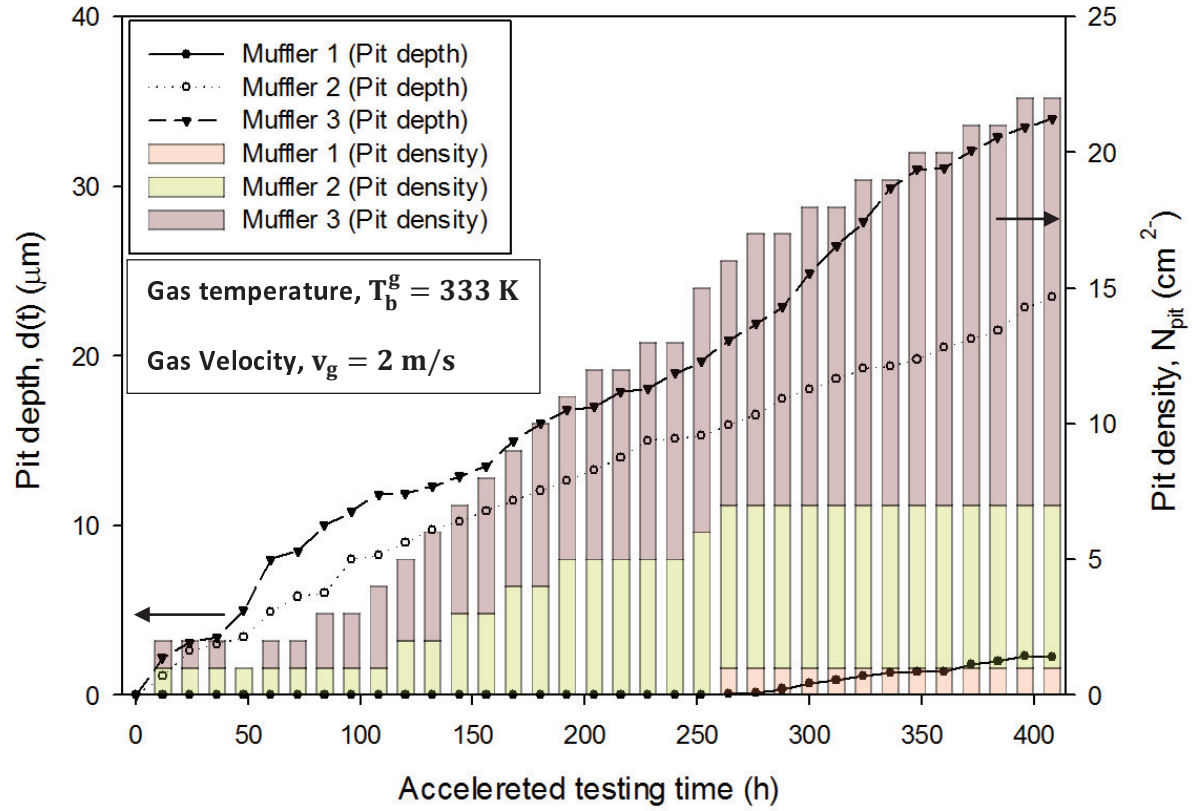

Figure 2 (a) The average wall temperature of three mufflers and corresponding condensation rates for each muffler with respect to accelerated testing time (b) The pit depth $\mathbf{d(t)}$, corresponding to pit density $\mathbf{N_{pit}}$, cm^{2-} for all the three mufflers due to corrosion

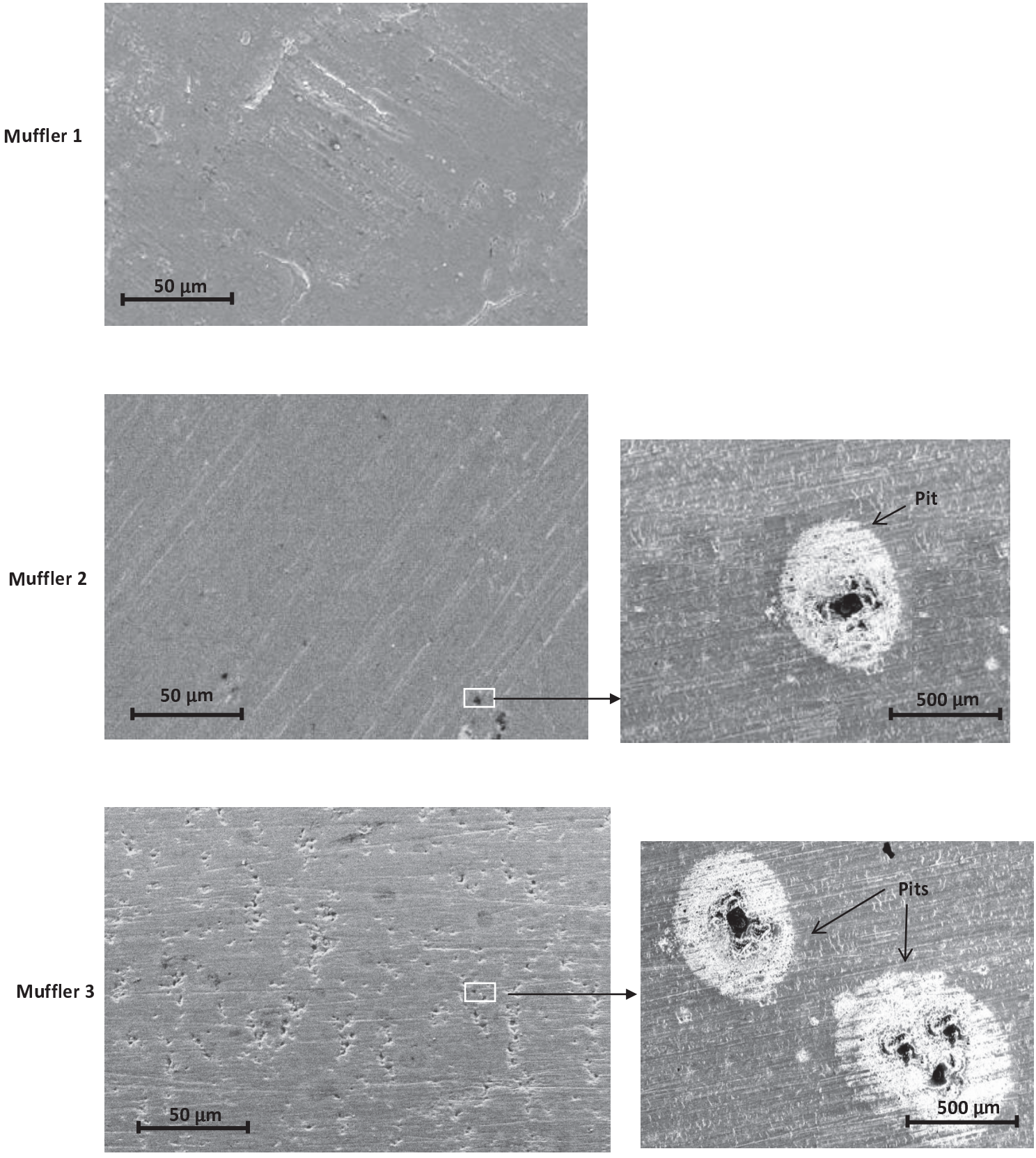

Figure 3. All the three mufflers were analysed using scanning electron microspore (SEM). The results showed highest pitting density in muffler 3, moderate in muffler 2 and least in muffler 1

(a)

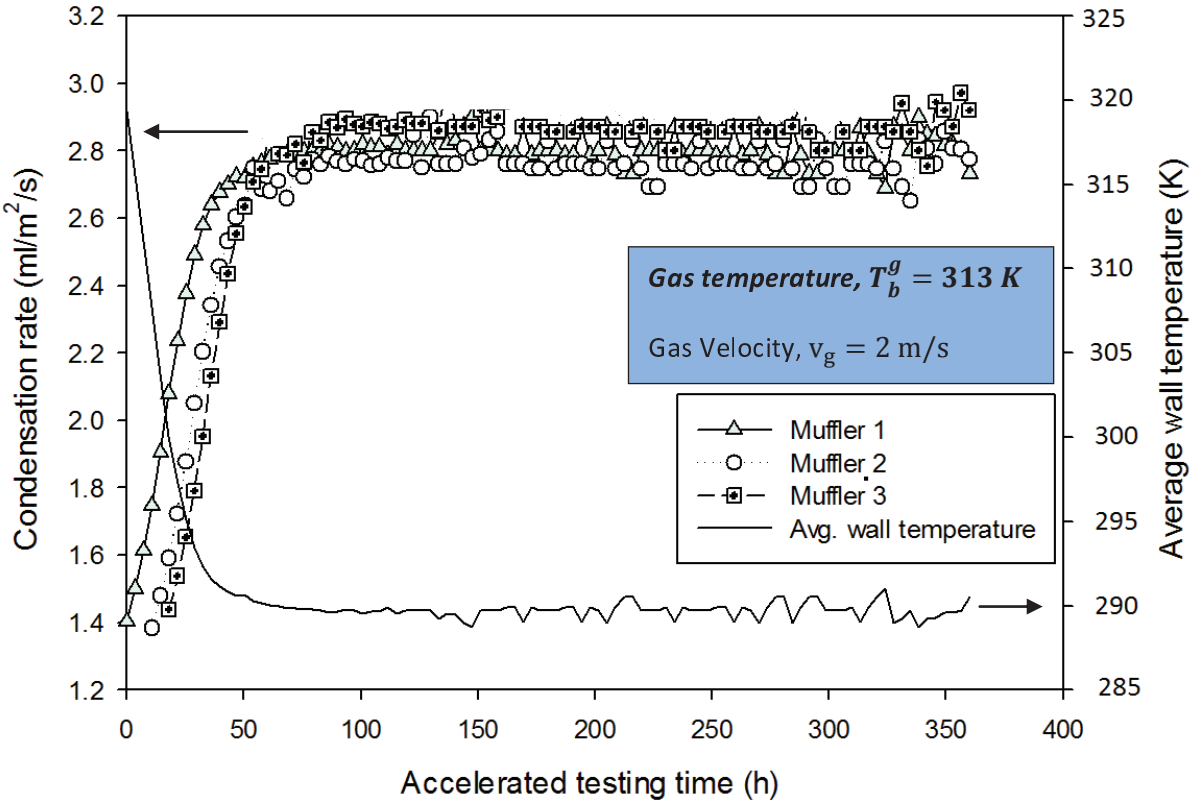

(b)

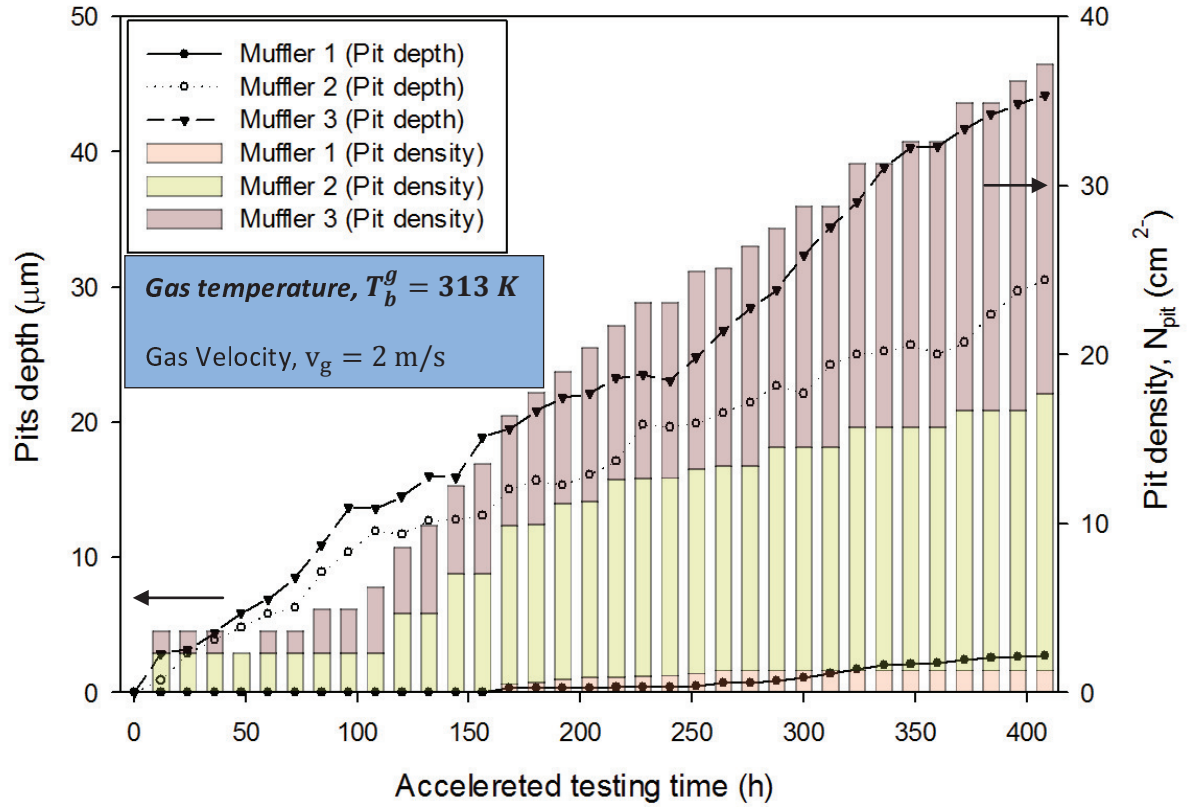

Figure 4. Condensation rates for each muffler with respect to accelerated testing time for the condition of low gas temperature 313 K. The trends are showing high condensation rates for low gas temperature (b) The pit depth $\mathbf{d(t)}$, corresponding to pit density $\mathbf{N_{pit}}$, cm^{2-} for all the three mufflers due to corrosion for condition of low gas temperature 313 K showing higher pitting corrosion rate (pit depth) in the mufflers

(a)

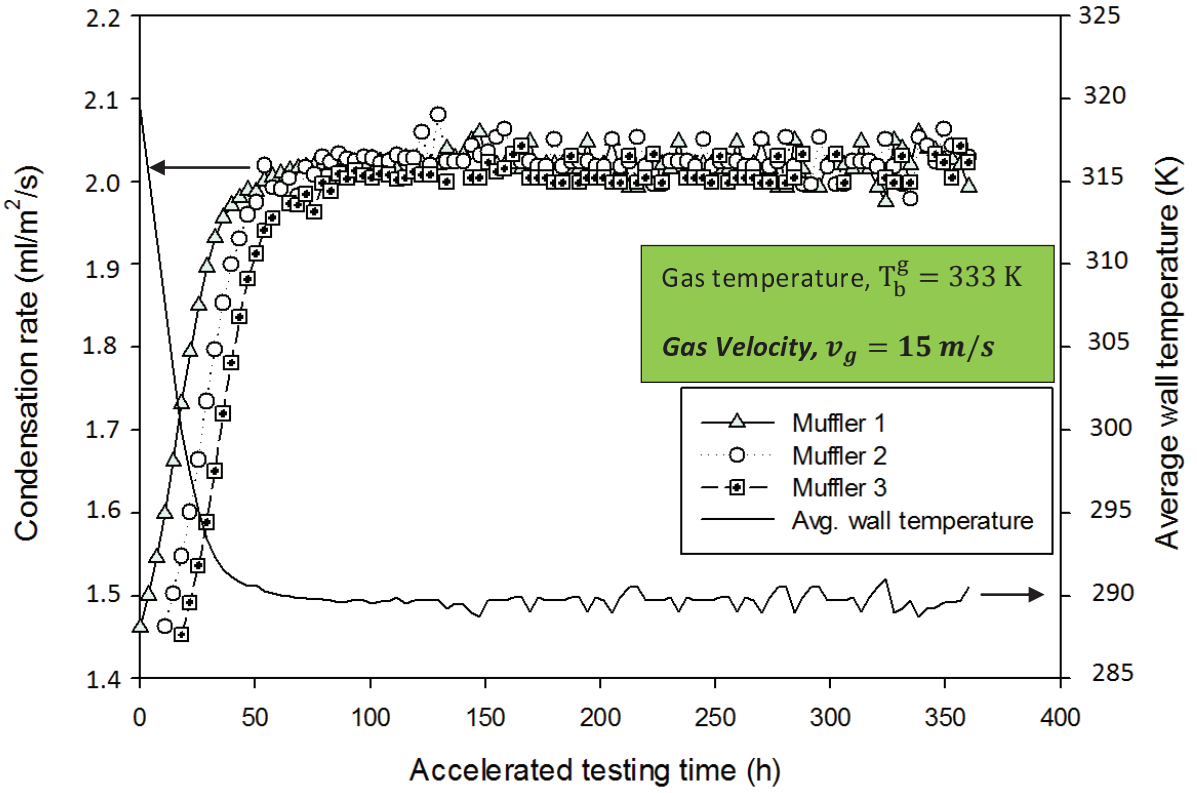

(b)

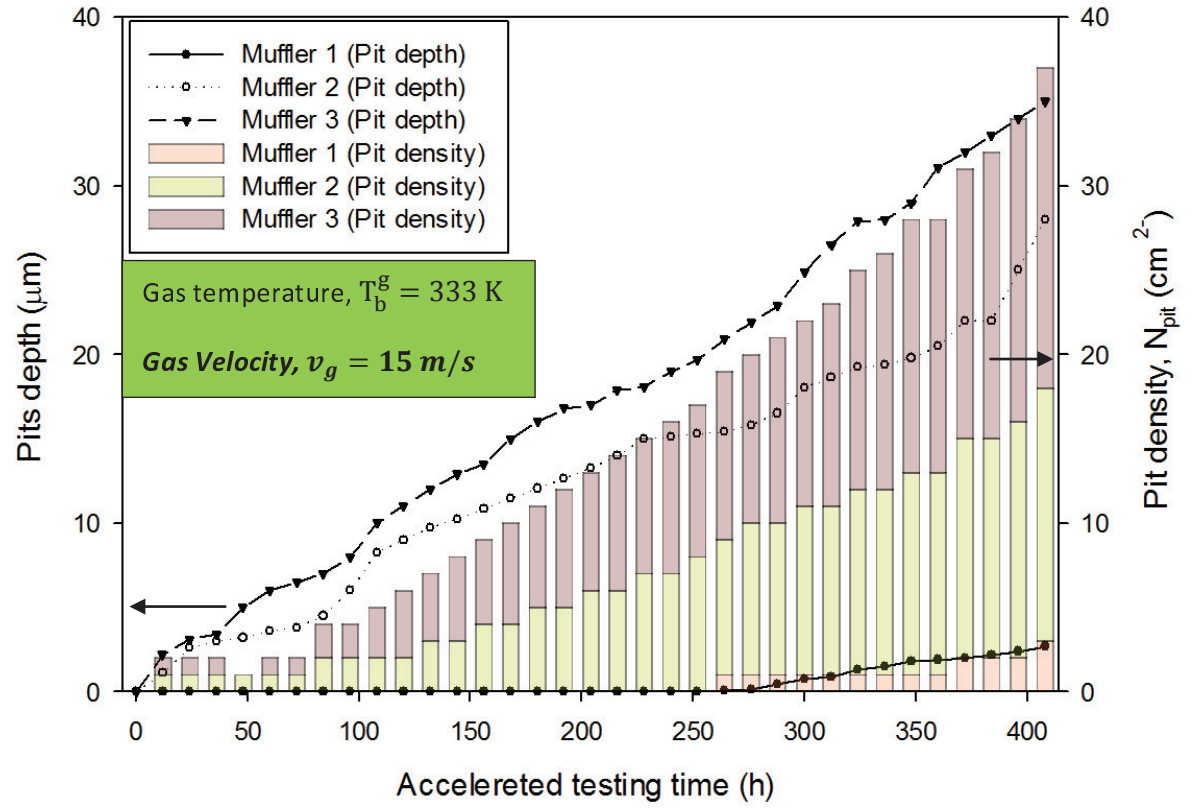

Figure 5. Condensation rates for each muffler for the condition of high gas velocity 15 m/s. The trends are showing high condensation rates for high gas velocity (b) The pit depth $\mathbf{d(t)}$, corresponding to pit density for condition of high gas velocity shows no significant high pitting corrosion rate (pit depth) in the mufflers compared to low gas velocity 2 m/s in fig, 2 (b).

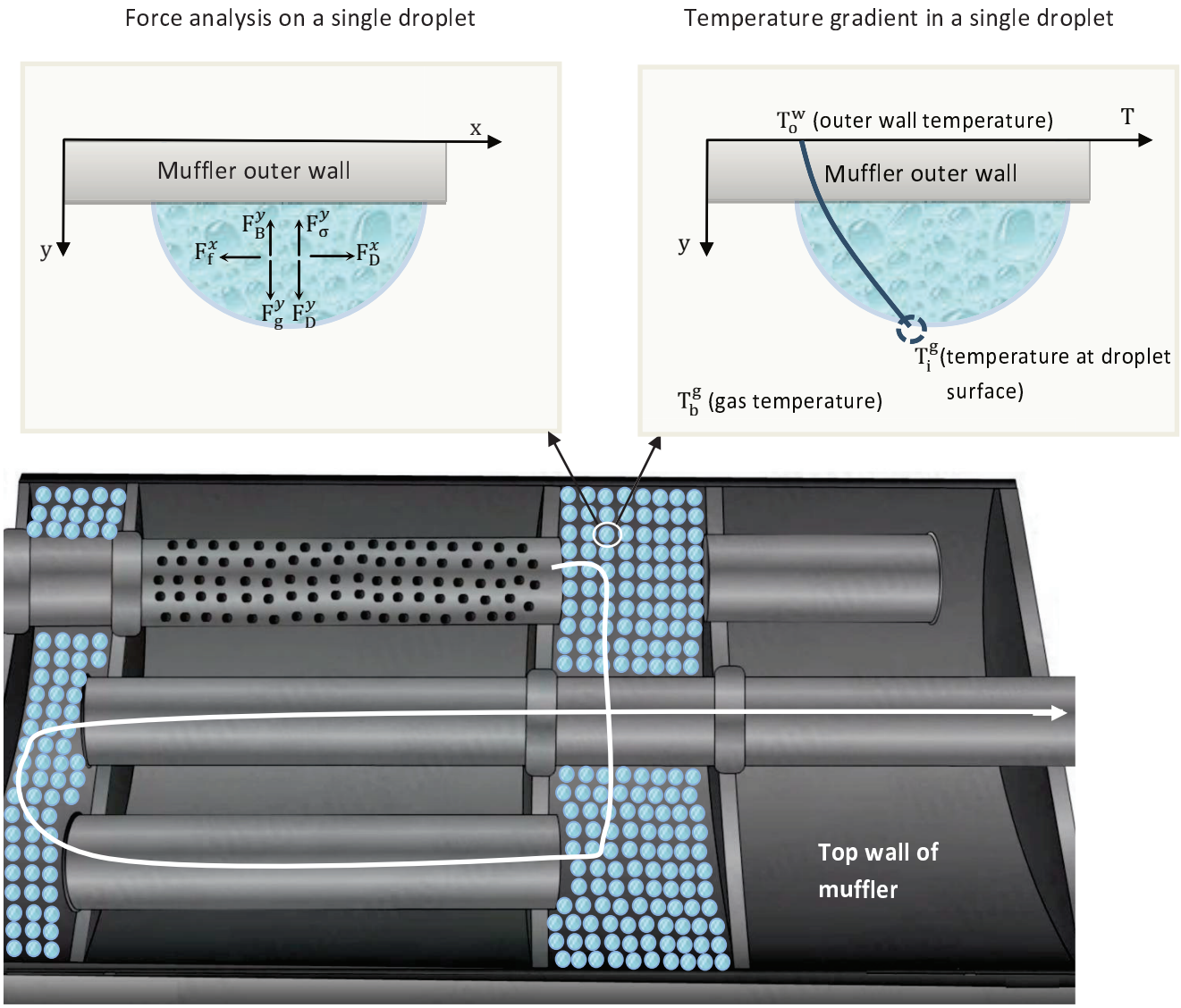

Figure 6. The drop wise condensation of water droplets on the top wall of muffler. The top left figure shows the force analysis on a single droplet; the top right figure shows the temperature gradient in a single droplet.

(a)

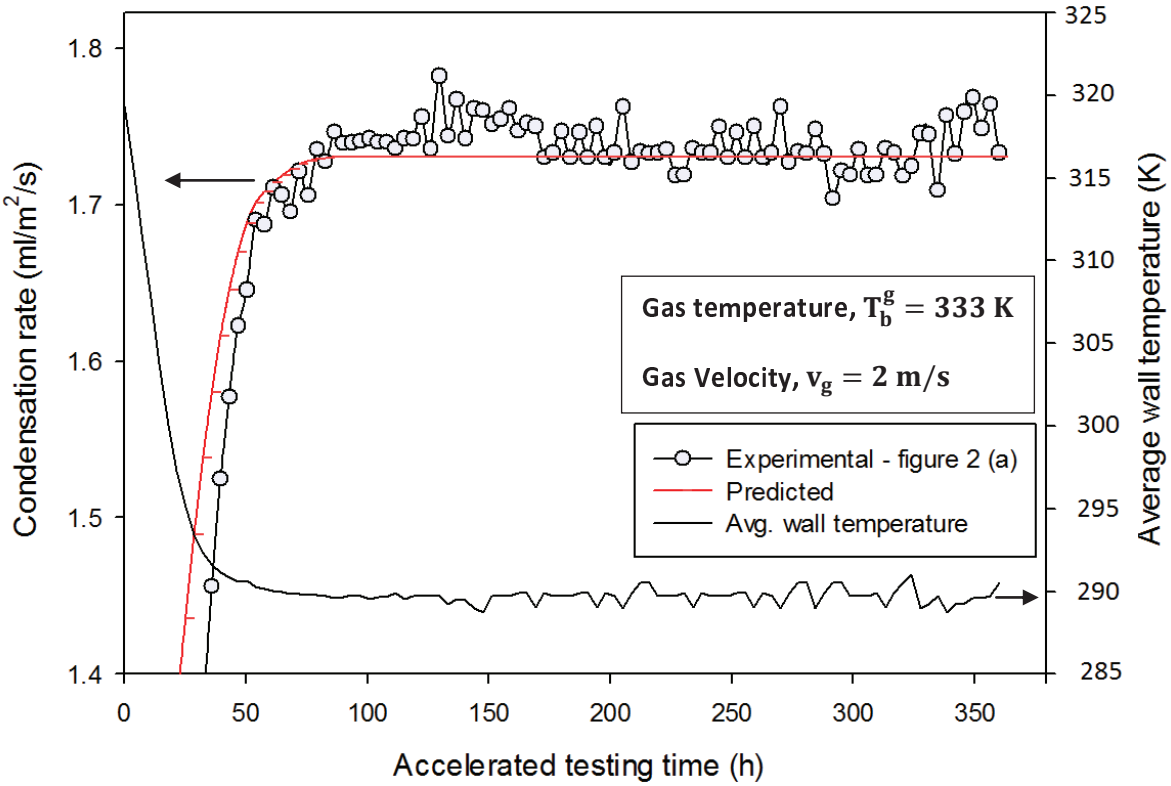

(b)

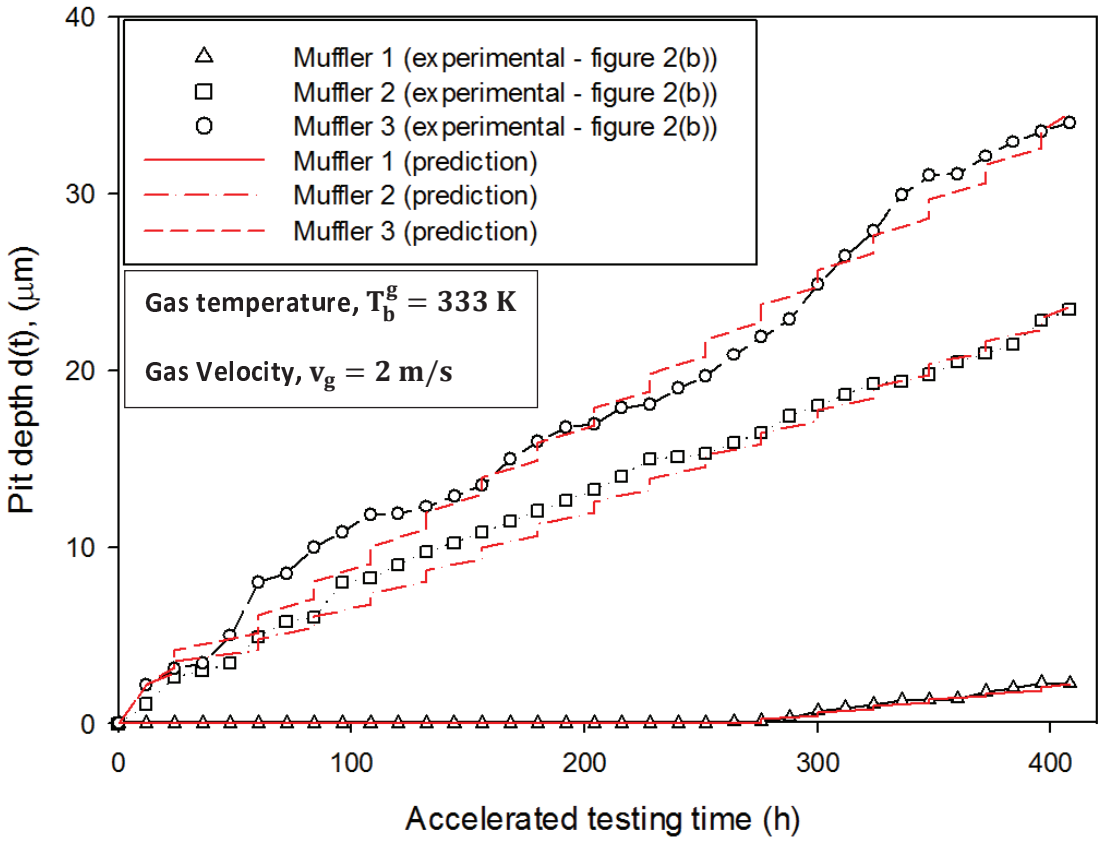

Figure 7. (a) The comparison between experiment and model prediction of condensation rate for decreasing wall temperature with respect to time for condition (b) Experimental and predicted trends for pit depth showing that it increases linearly with the passing time (hours). The 'stair-case' appearance in predicted results is due to the many droplets that form, grow and detach during the course of the simulation, each "fluctuation or step" representing droplets lifetime.

(a)

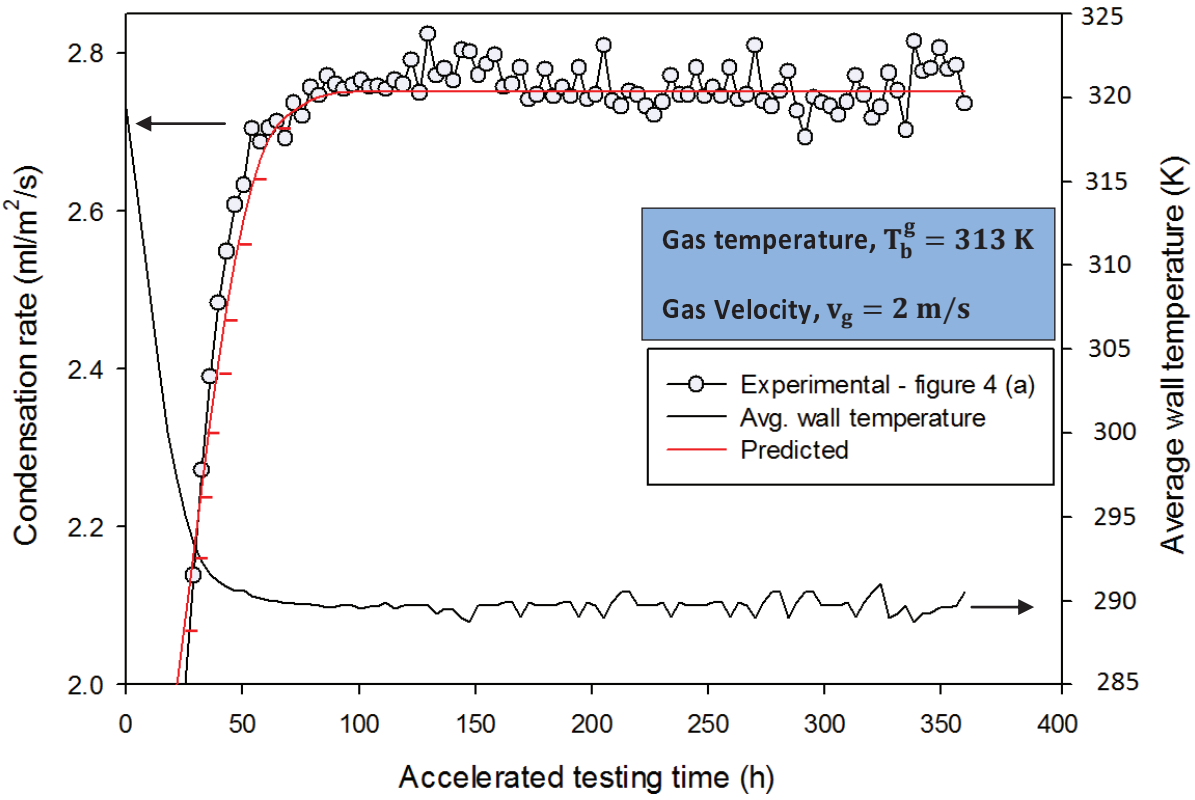

(b)

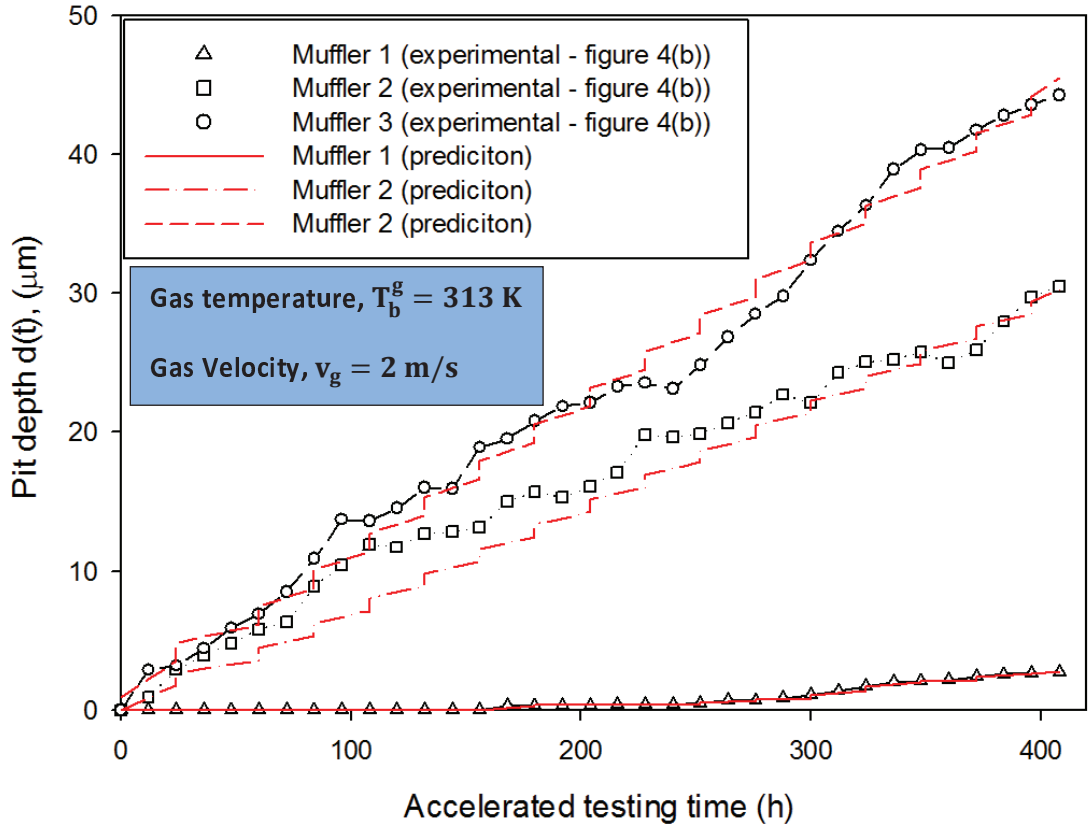

Figure 8 (a). Condensation rate for condition of low gas temperature 313 K. (b) Corrosion rate (pit depth) showing that the resultant pit depth increases with time. The trends show a good agreement between predications and experimental results

(a)

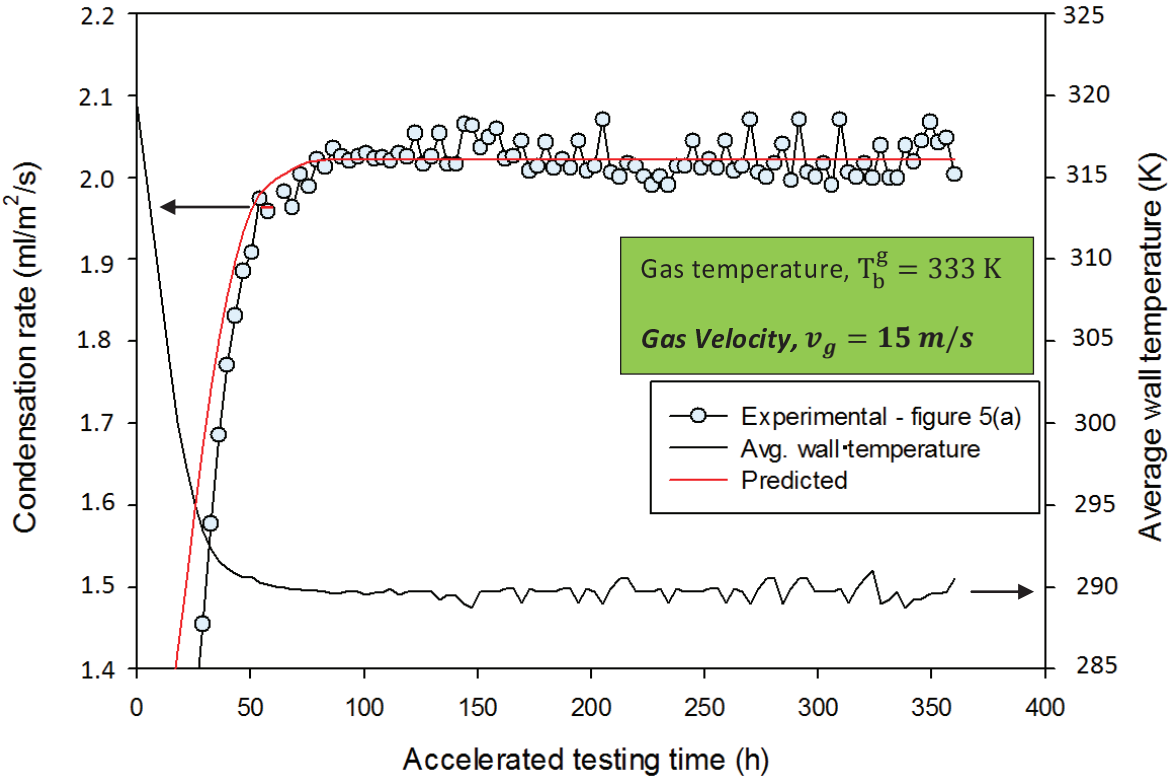

(b)

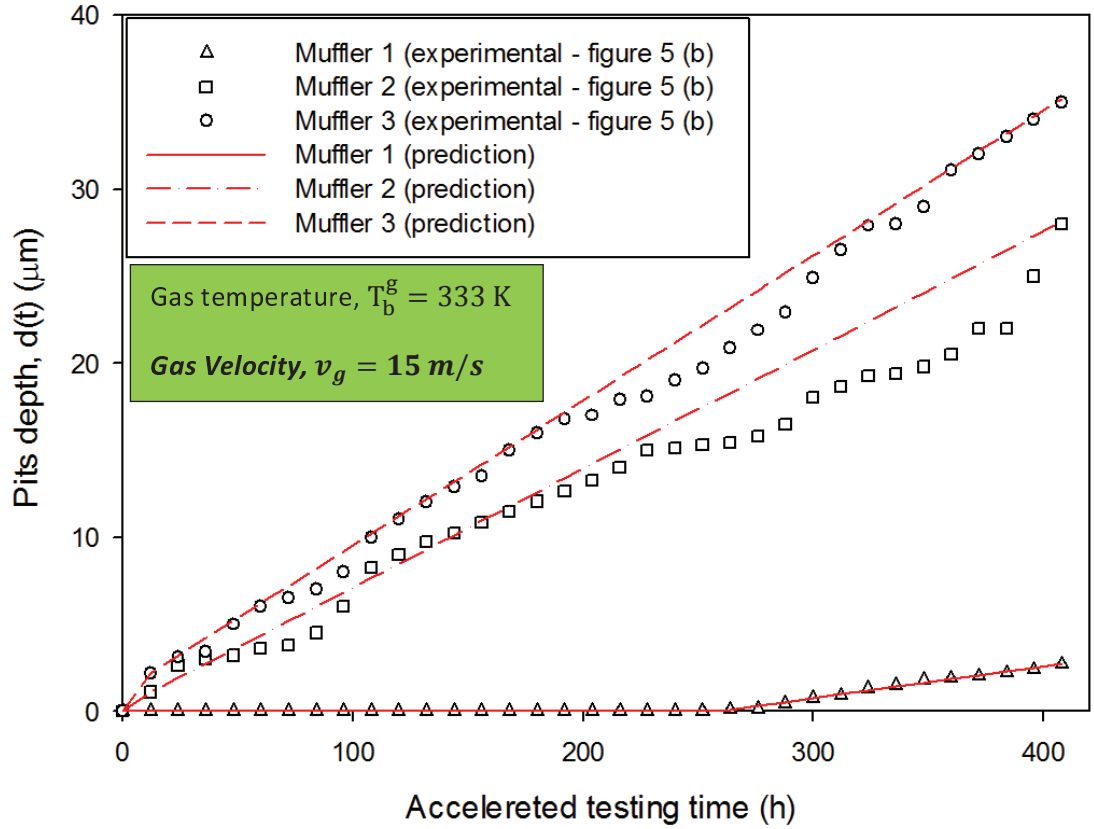

Figure 9 (a). Condensation rate for condition high gas velocity v_g = 15 m/s compared to low gas velocity v_g = 2 m/s showing high condensation rate with respect to time compared to low gas velocity (b) Corrosion rate (pit depth) does not show a major change compared to low gas velocity. It is worth noting that the 'stair-case' situation, now becomes straight line for high gas velocity

Tables

Table 1. The exhaust gas composition for each muffler. The exhaust gases with these compositions were allowed to pass through muffler 1, 2 and 3.

Compound	Exhaust gas composition		
	Muffler 1 (%)	**Muffler 2 (%)**	**Muffler 3 (%)**
Nitrogen	78	67	71
Carbon dioxide	-	12	14
Water vapour	< 1	11	12
Oxygen	21	10	3
Trace elements	-	~ 0.3	~ 0.5
Nitrogen oxides	-	~ 0.15	~ 0.25
Carbon monoxide	-	< 0.045	~ 2
Hydrocarbons	-	< 0.03	< 0.25
Sulphur dioxide	-	< 0.03	< 0.2

Table 2. The condensate from three mufflers is collected to perform pH and chemical trace analysis (CTA). The CTA is performed to evaluate the condensate composition showing that the condensate is composed of chloride ions Cl^-, sulphate ions SO_4^{2-}, carbonate ions CO_3^- , and nitrate ions NO_3^-.

Exhaust gas condensate composition					
Muffler 1		**Muffler 2**		**Muffler 3**	
pH	~ 6	pH	4	pH	3
$[Cl^-]$	-	$[Cl^-]$	75 ppm	$[Cl^-]$	160 ppm
$[SO_4^{2-}]$	-	$[SO_4^{2-}]$	200 ppm	$[SO_4^{2-}]$	500 ppm
$[CO_3^-]$	-	$[CO_3^-]$	120 ppm	$[CO_3^-]$	300 ppm
$[NO_3^-]$	-	$[NO_3^-]$	6 ppm	$[NO_3^-]$	10 ppm